Heritage Science

RESEARCH

Open Access

Glass beads from a Scythian grave on the island of Khortytsia (Zaporizhzhia, Ukraine): insights into bead making through 3D imaging

Dmytro Nykonenko[1,2*], Oleh Yatsuk[1], Laura Guidorzi[3,4], Alessandro Lo Giudice[3,4], Francesca Tansella[3,4], Ludovica Pia Cesareo[3,5], Giusi Sorrentino[3], Patrizia Davit[1], Monica Gulmini[1] and Alessandro Re[3,4]

Abstract

Four glass beads from a Scythian burial on the island of Khortytsia (Southern Ukraine) were subjected to 3D imaging using micro-CT and photogrammetry. The aim was to reconstruct the process used to produce and decorate the beads by detecting and interpreting the traces left by the technological processes on the bead surface and in the glass body. It turned out that all the beads were obtained by winding hot glass around the mandrel. The distribution, size and shape of the bubbles in the glass matrix revealed by the micro-CT scans and the features observed during a thorough examination of the photogrammetric models allowed us to follow the movements of the bead maker during the formation of the bead body and its decoration, highlighting several details of the production processes such as the number of the superimposed layers and the direction of the rotation of the mandrel during both the formation of the body and the decoration of the bead. Some information about the tools also emerged, with particular reference to the shape of the mandrel, the possible use of a releasing agent and how tools were used to decorate the surface or to remove the beads from the mandrel. According to the archaeological classification, the beads considered here belong to three different types, that are considered chronological indicators of the fourth century BCE and are found in archaeological sites spread over an area extending for several thousand kilometers from the Black Sea coast to the Ural Mountains. This work enriches the knowledge of the micromorphology of beads found in Eastern Europe, which is rarely discussed in the scientific literature on the archaeological glass beads.

Keywords Glass beads, Fourth century BCE, Scythian culture, Micro-CT scan, Photogrammetry

Introduction

Glass beads are common finds in archaeological sites from prehistory to modern times, and through the combination of archaeological and archaeometric inferences they provide insights into the economic, social and cultural contexts as they are relevant markers of regional and long-distance exchange and relationships [1–6].

Archaeologists typically rely on typological categories to describe and classify the glass beads, which allows the comparison of the finds retrieved from different archaeological contexts according to a defined hierarchy of attributes obtained through close observation [7–10].

*Correspondence:
Dmytro Nykonenko
dmytro.nykonenko@unito.it
[1] Department of Chemistry, University of Turin, Via Pietro Giuria, 7, 10125 Turin, Italy
[2] Khortytsia National Reserve, Vulytsya Starogo Redutu 9, Zaporizhzhia 69017, Ukraine
[3] Department of Physics, University of Turin, Via Pietro Giuria, 1, 10125 Turin, Italy
[4] Istituto Nazionale di Fisica Nucleare (INFN) Sezione di Torino, Via Pietro Giuria, 1, 10125 Turin, Italy
[5] Department of Environmental Sciences, Informatics and Statistics, Ca' Foscari University, Via Torino, 155, 30172 Mestre, VE, Italy

The literature also reports how to describe the so-called "defects in the glass mass", with particular attention to gaseous, vitreous and non-vitreous inclusions [11].

From an archaeometric point of view, the chemical composition of a glass bead reflects the materials that were used to prepare the bulk of the glass, to color it, or to induce opacity, possibly in a sequence of operations not necessarily performed in the same place [12, 13]. Compositional fingerprints can therefore help to trace the origin of the raw materials and then identify (or at least suggest) where the glass-making/glass-working took place [14–17].

The microstructure of the bead, mainly in terms of the number, shape, orientation and distribution of voids and crystalline inclusions in the glass matrix, preserves the traces of the processes used by the bead maker and testifies to the very moment of the bead creation, when the glass was shaped/assembled to create the final object.

In principle, both chemistry and (micro-)morphology can contribute some knowledge to reconstruct the production history of the glass objects, providing valuable information for tracing their origin. Therefore, a deeper insight into ancient glass technology and exchange networks is possible by combining these approaches [18, 19].

Several bead-making techniques have been used in the past. When glass is coiled (wound) around the mandrel one or several times the resulting beads are called wound beads. If glass is made into a tube and stretched in the direction of the aperture with subsequent cutting off the segments, the resulting beads are called drawn beads. Beads can also be made by using various molds or folding glass [3, 8, 9, 20–23]. Often glass beads are decorated with other kinds of glass that make a pattern. Decorative elements on beads have their own techniques of application.

The bead-making process has its most evident effect on the orientation and shape of the bubbles trapped in the glass matrix [3, 22, 24]. Elongated bubbles oriented perpendicular to the hole are typical for wound and folded beads, while elongated bubbles parallel to the aperture are expected for drawn beads [8, 25]; molded beads typically lack orientation or elongation in their bubbles. In addition to these general expectations, it should be noted that further processing of the bead at high temperatures, such as for decoration or further shaping, may affect the orientation or shape of the bubbles, and even remove them completely. Finally, the shape and dimensions of the aperture will reflect those of the mandrel used to produce the bead.

Unfortunately, the search for detailed information about the bead-making technique through the study of micromorphology is rarely the focus of research, mainly because the features are difficult to capture and to document either by unaided visual observation or with affordable instrumental techniques. As a result, while typological discussions and chemical analyses have provided a significant support for discussion in archaeology [2, 4, 8, 9, 12, 13, 21, 26, 27], the literature contains far fewer papers that would allow the glass beads to be examined beyond their appearance and composition, highlighting differences and similarities between beads in addition to the typological and compositional approach.

In order to contribute some new knowledge to this topic, we considered a set of glass beads from a Scythian burial. The grave is located on the island of Khortytsia in the Dnipro River (city of Zaporizhzhia, Southern Ukraine) and is part of the cemetery called "Kanfarka". The cemetery dates back to the fourth century BCE and, in contrast to the widespread Scythian barrow burial structures, it is a relatively rare type of cemetery, in which the graves were not covered by earth mounds [28]. This cemetery is one of the many monuments of the Scythian period on the island of Khortytsia. This large island was one of the few places of convenient crossing points between the banks of the Dnipro River, and it was located at the end of the waterway connecting the deep steppe regions with the Black Sea and the Greek colonies. Thus, it was situated at the busy crossroads of trade and nomadic routes of great strategic importance.

The beads were found in the burial No. 5, which was unearthed in 2021. The burial was made in a shallow pit with a recess oriented along the west–east axis and not marked on the surface by any stone structures traditional for the site. The grave was looted in ancient times and only an iron knife with a bone handle and 12 glass beads remained among the burial goods. Because of the robbery, which moved the objects from their original place and, possibly, took away part of the assemblage, it is impossible to know the original number of the beads in the burial and their functional use. We divided the surviving beads into four types and one bead of each type is included in this study.

The beads have direct analogies in the inventory of other burials in the Kanfarka cemetery [29]. They also have numerous analogies in the archaeological sites of various nomadic cultures known along several thousand kilometers from the Black Sea coast to the Ural Mountains [30–33]. Some of these glass beads are reliable chronological indicators of the fourth century BCE, despite the different cultural affiliations of the archaeological sites themselves in such a large area [34]. They usually come from female burials, and only a few examples are found in male graves. They were worn on the neck, arms, and legs and were often arranged in the same color scheme [35].

According to Alekseeva's classification, which was thoroughly developed for glass beads from the Northern Black Sea region, the beads presented here belong to the general group of polychrome glass beads [30, 35]. Within this group, the author distinguishes 400 types of beads based on ornament, shape, color, opacity, and manufacturing techniques. The beads included in this study are briefly described in Table 1. The colour given in the table and throughout the text is that observed macroscopically. The black colour may be due to intensely coloured chemical species, which cause the bead to appear black due to the thickness of its vitreous mass. Additional file 1: Fig. S1 provides images of the beads from an archival documentation perspective.

Initially, the set of the four selected beads was examined under a stereomicroscope equipped with a digital camera, in order to capture the most prominent morphological features appearing at different angles of (visible) illumination. Then, they were subjected to micro-X-ray computed tomography (CT), photogrammetry and scanning electron microscopy coupled with energy dispersive spectrometry (SEM–EDS).

CT is among the most powerful 3D modeling techniques currently used in archaeology [5, 36], given its capability of investigating the inner parts of an artefact in a non-invasive way. Employed at first only as a medical diagnostic tool, its potential has been quickly recognized and its use has been extended to different research areas, where some limitations—such as radiation dose restrictions—could be overcome. New setups like industrial scanners entered the scene, and with the use of high brilliance sources such as synchrotron radiation, acquisition times could be drastically reduced [37]. CT scan has been utilized in archaeology mainly to examine mummies and skeletal remains [38–40] and for the non-invasive inspection of blocks of soils embedding fragile archaeological relics [41]. In addition, CT scan can support the archaeological research for a wide variety of materials and archaeological objects: some of them are very usual and widespread, such as ceramic and clay for pottery and clay tablets [42, 43], metal for coins, weapons and tools [44, 45], wood for coffins, boats and musical instruments [46–48] while others are rarer and less common, such as shell beads [49] and birch bark tar [50]. CT is undergoing continuous technological improvements and refinements in data analysis, focusing in particular on portability [51, 52], adaptation to specific materials or shape requirements [53–55] and optimization of reconstruction and segmentation methods [56, 57]. This process is leading to an increasingly broad application of the technique in the field of cultural heritage, extending to new types of objects and materials that have never or only marginally been studied with X-ray CT.

As for glass beads, by capturing the interior elements in addition to surface features, micro-CT can detect bubbles and inclusions, reveal the detailed morphology of the hole and of the decoration, and highlight any other feature showing sufficient X-ray attenuation contrast to be detectable within the boundaries of the instrumental resolution [3, 5, 22, 24]. Authors of these publications discuss the bead-making techniques trying to get a deeper insight into the production methods. However, for the analysis of such samples, it is necessary to take into account some issues during the acquisition and the data evaluation, such as the need to avoid radiation damage, that can induce color changes in the glass [22]. Moreover, care must be taken to correctly identify X-ray artifacts to avoid their misinterpretation [5]. Finally, it may sometimes be impossible to distinguish different materials (such as inclusions of decorations) based on gray scale values alone.

In addition to the CT scan, which is able to image the entire volume of the bead, we used photogrammetry to create a 3D model reconstructing the geometry of the beads and the texture of the surface. The use of photogrammetry in the field of cultural heritage has been widespread since the end of the last century [58]. Thanks to significant improvements in the software over the last few decades, its use is now ubiquitous [59–61]. In the vast majority of its applications on archaeological objects, photogrammetry is used to document the appearance of the objects. In this paper, however, we focus on the strength of this technology for research purposes. First of all, we faced the task of creating measurably accurate 3D

Table 1 The beads involved in this study

Lab. Id	Type [ref.]	Description	Diameter (mm)	Length (mm)
KH1	276 B	Cubic black opaque bead with yellow chevron decoration	16.7	12.5
KH7	203 B	Barrel-shaped opaque green bead with one yellow stripe on the largest perimeters	14.5	21.2
KH8	203 B	Barrel-shaped opaque black bead with one yellow stripe on the largest perimeters	13.7	15.5
KH11	13	Round, slightly flattened opaque black bead, with even white, yellow and red spots	16.2	12.5

Type refers to the classification given in [27, 32]. Dimensions are given according to [7]. The black colour is what appears under macroscopic observation

models of glass beads, allowing us to analyze the surface of objects, their color and texture variations. It is worth noting that the application of photogrammetry to glass objects in general [62], and to glass beads in particular [63], is not trivial. These difficulties lie in the intrinsic characteristics of glass as a material, such as its reflective properties and its translucency/transparency. In the case of beads, the small size and the presence of certain hard-to-reach areas, such as the inner surface of the hole, are also significant issues.

We also explored the new possibilities offered by the synergy between photogrammetry and micro-CT, beyond the already proposed application of 3D digitization of complex glass objects for archival recording [64]. The combination of the point clouds extracted by thresholding a CT volume and the one obtained directly by photogrammetry into one single 3D model allows the simultaneous analysis of the textured, colored surface and of the internal microstructure, thus supporting the interpretation of the overall features with respect to ancient bead making processes.

Finally, to complement the morphological approach, Scanning Electron microscopy coupled with energy dispersive spectrometry (SEM–EDS) was employed under low-vacuum conditions to (qualitatively) characterize the base glass and the high-Z materials that were used to give colors to the decorations.

The goal was to obtain an insight into the micromorphology of these types of glass beads, which are relevant markers of exchange in the fourth century BCE in a wide area north of the Black Sea coast.

Instruments and procedures

Stereomicroscope

The samples were observed under a Leica 12.5 stereomicroscope equipped with a 1× planar apochromatic objective and two 10× ocular lenses, mounted on a LED2500 stand with integrated illumination with four angles for the incident light to enhance contrast on the surface. The stereomicroscope is coupled with a MC 190 HD digital camera with 10 megapixel CMOS sensor managed by the LAS X software. All the equipment and the software are from Leica Microsystem (Wetzlar, Germany).

Scanning electron microscopy coupled with energy dispersive spectrometry (SEM–EDS)

The beads were placed in the sample chamber of a JEOL (Tokyo, Japan) JSM IT300LV electron microscope equipped with an INCA X-act SDD thin window energy dispersive X-ray detector from Oxford Instruments (Abingdon, UK) managed by the AZtecLive software platform, with the aim of obtaining, in low vacuum conditions (50 Pa), the qualitative composition of the base glass and of the decorations. The surface of the bead was also documented through BSE images.

Micro-CT system

The tomographic system for data acquisition has been developed by the Physics Department of the University of Torino and the INFN (Italian National Institute for Nuclear Physics) and is described elsewhere [48]. Its main components are a Hamamatsu (Hamamatsu City, Japan) Microfocus L8121-03 X-ray source, a Newport (Irvine, California, USA) URS150BPP rotation stage and a Shad-o-Box 6 K HS Flat Panel detector from Teledyne Dalsa (Waterloo, Ontario, Canada). In this set scans, the system alignment was accomplished by manually controlling the vertical movement of the source and the angular tilt of the rotation stage, while the detector was finely moved horizontally and vertically by remotely controlling the two mechanical axes on which it was mounted. The geometry of the setup and the X-ray beam characteristics were optimized taking into account the type of the material and the dimensions of these specific glass beads, as shown in Table 2. The projections were acquired through a custom NI (Austin, Texas, USA) Labview routine that synchronizes the rotation motion and the projection acquisition. The same routine was used to acquire 20 "open-beam" images (same conditions, no sample) and 20 "dark" images (X-rays off), which were averaged using MATLAB software.

Table 2 Experimental parameters for the CT acquisitions

Parameter	Value
Tube voltage	150 kV
Tube current	66 µA
Focal spot size	7 µm
Filtration	Al (2 mm)
Detector pixel size	49.5 µm
Detector pixel number	2304 × 2940
Detector active area	11.4 × 14.6 cm^2
A/D converter	14 bit
Integration time	1.8 s
Angular step	0.15°
Number of projections	2400
Average time for a CT scan	150 min
Source-Detector Distance (SDD)	650 mm
Source-Object Distance (SOD)	120 mm
Object-Detector Distance (ODD)	530 mm
Magnification	5.4×
Voxel size	9.1 µm
Penumbra	31 µm
Scanned volume diameter	21 mm
Scanned volume height	27 mm

The following software was used for CT reconstruction and visualization:

- ParRec, a parallel research software developed by the University of Bologna (Italy) [65] for flat-field correction and CT reconstruction, obtained using a Feldkamp, Davis and Kress (FDK) algorithm with cone-beam geometry [66];
- ImgRec, a non-commercial software utility developed by Dan Schneberk of the Lawrence Livermore National Laboratory (Livermore, CA, USA) [65], for ring artifact correction on sinograms;
- ImageJ [67] for the visualization of the image sequences and basic handling of projections and CT slices;
- Dragonfly (version 2022.1, ORS Inc., Montréal, QC, Canada) and VGStudio Max (version 2.2, Volume Graphics GmbH, Heidelberg, Germany) for the 3D rendering of CT volumes, segmentations, dimensional measurements and for exporting the point-clouds. Structural features of the beads were differentiated by the brightness level of the voxels (related to relative density and Z-number). Maximum Feret diameter, measured by an algorithm implemented in the software as the longest distance between two parallel tangents along the object's convex hull, was used for the dimensional classification of gaseous inclusions.

Photogrammetry

The photographs used to create the 3D models were taken with a Canon EOS 5DS R camera (Tokyo, Japan) using a Zeiss Milvus 50 mm f / 1.4 ZE lens (Oberkochen, Germany). The JJC EF/EF-S mount 12 mm adapter (Shenzhen, China) was used to enlarge the object in the image. The images were taken under manual focusing conditions, using a turn table and a tripod. A specially designed metal plate with a laser-applied coordinate grid was used to build a local coordinate system [68]. The plate is made of ST3 grade steel (thermal expansion coefficient: 9.9 microns per 1 C° per meter), the grid size is 150×150 mm, and the application accuracy is 50 microns.

The equipment was operated using the Canon Camera Connect v3 remote imaging software (Tokyo, Japan). The optical distortion of the RAW images was corrected in the Camera RAW v14.1 plug-in for Adobe Photoshop software (San Jose, U.S.A.). The Agisoft Metashape v1.8.1 software was used to create 3D models, which are available at the Sketchfab platform website [69]. The CloudCompare v.2.12.4 open source software was used to combine different point clouds obtained by photogrammetry and micro-CT.

Results

Microstructure of the surface and composition of the glass

Optical and electron microscopy revealed several features of the surface, all of which could be reproduced in the photogrammetric models.

Figure 1 shows some representative examples, such as the corrugation that appears in KH1 (Fig. 1, A1–A3), the dense network of cracks that gives the surface of KH7 a "sugary texture" (Fig. 1B1–B3), the evident traces of the winding in KH8 (Fig. 1C1–C3), and the wrinkled texture that characterizes the surface of KH11 (Fig. 1D1–D3). In all the bead types considered here, the glass used for decorations features a higher porosity than the glass used to form the bead. The higher spatial resolution of the scanning electron microscope would also provide an even deeper insight into the state of preservation of the glass surface, highlighting pitting and traces of corrosion (not shown) [70].

Electron microscopy coupled to energy dispersive spectrometry also allowed us to obtain some information about the composition of the glass. Since the analyses were carried out using a non-invasive approach in low-vacuum conditions, we expect that the data do not represent the actual composition of the bulk glass, but that of the alkali-depleted surface, possibly contaminated by the burial environment [71, 72].

Nevertheless, some information emerged from the analyses. There was no evidence of elevated potassium concentrations, so we could reasonably assume that all the glasses used for the formation of the beads considered here are soda-lime. KH11 contains a high concentration of iron, which would explain the black colour, although such an elevated concentration could not be found for the other types of black beads considered here. The green color of KH7 is related to the presence of copper in the glass matrix. As for the decorations, elemental analysis suggests that both the white and the yellow decoration are based on antimony compounds, while the origin of the red color of the embedded dots in KH11 is not clear, as significantly high levels of both iron (which, in principle, can give red as dispersed crystals of hematite) and copper (which gives red both in the form of elemental copper and of cuprite crystals) were detected.

Microstructure of the body

The results of CT scans are presented as slices in both the longitudinal (parallel to the aperture) and axial (perpendicular to the aperture) directions, highlighting the most prominent features in the four beads. Figure 2 shows two representative slices for each of them. The grayscale

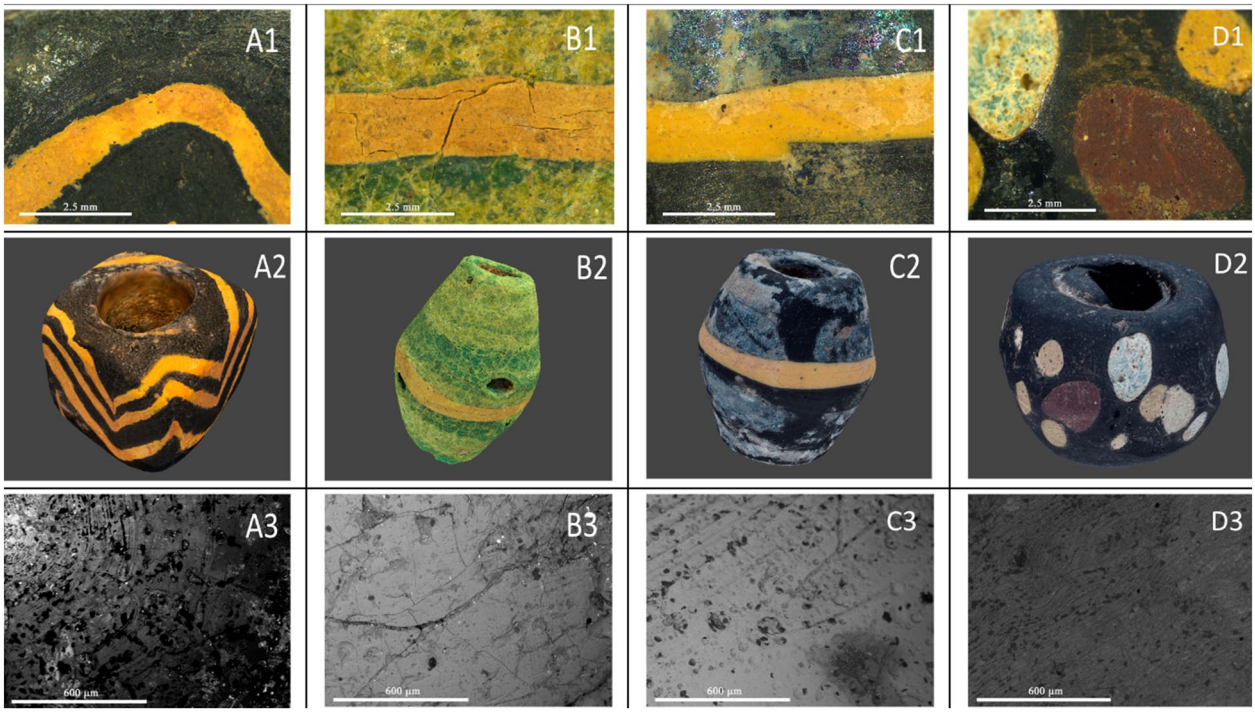

Fig. 1 Columns from left to right show details for KH1, KH7, KH8 and KH11 obtained: 1) with optical stereomicroscopy (scalebars 2.5 mm); 2) by 2D images from the photogrammetric 3D models; 3) by back-scattered electron microscopy (scalebars 600 µm)

images reflect the X-ray attenuation coefficient, linked to the density and the atomic number (Z) of the material, therefore the darker voxels are related to gaseous inclusions and the brightest ones are related to the decorations, for which high Z-value compounds were used (see Sect. "Microstructure of the surface and composition of the glass").

First of all, it was possible to highlight a high variability in both shape and dimension of the bubbles entrapped in the glass matrix. The main processes leading to bubble formation in glass beads have been reviewed by Bertini el al. [22], who attributed the origin of "seeds" (tiny bubbles less than 100 µm in diameter) to chemical reactions between glasses of different composition, and that of the larger bubbles to the deposition of furnace dust particles acting as nuclei, or to the entrapment of gasses when layers of glass are superimposed. The shape of the larger bubbles can be influenced by the movements made by the soft glass during the creation of the bead, and then retain the distorted shape because of the rapid stiffening of the glass.

All the four beads considered here showed some traces of the winding technique, with elongated bubbles in the direction of rotation (Fig. 2). Both CT-scan projections demonstrate no evidence of the fold passing through the objects. This allows to exclude folding (bending) as the production technique for these beads [23]. In addition to the highly radiopaque decorations, the slices highlight the presence of low-Z inclusions, possibly representing crystalline residues from the glass-forming raw materials. Moreover, sporadic high-Z small particles were also detected in the body of the beads. The network of cracks already evident on the surface of KH7 revealed to extend throughout the bead, and a high heterogeneity of the internal glass characterizes the internal structure of KH8 (Fig. 2).

Finally, the (more or less thick) layer of porous materials that was visible in the internal part of the perforation was clearly highlighted in the CT scans (Fig. 2 and Fig. 3).

In order to better visualize the different features through 3D models, their segmentation was performed by setting different threshold values for the gray levels in Dragonfly. This allowed us to extract from the 3D rendering the features that fell within a specific range of gray levels, thus separating different components such as bubbles, low-Z inclusions, high-Z inclusions and the decorations. The choice of the threshold was tailored for each bead by carefully studying the results of the segmentation on the sequence of transverse and radial sections. The point clouds obtained by segmenting the CT volumes are valuable tools to reconstruct the bead making technology for each of the beads considered here.

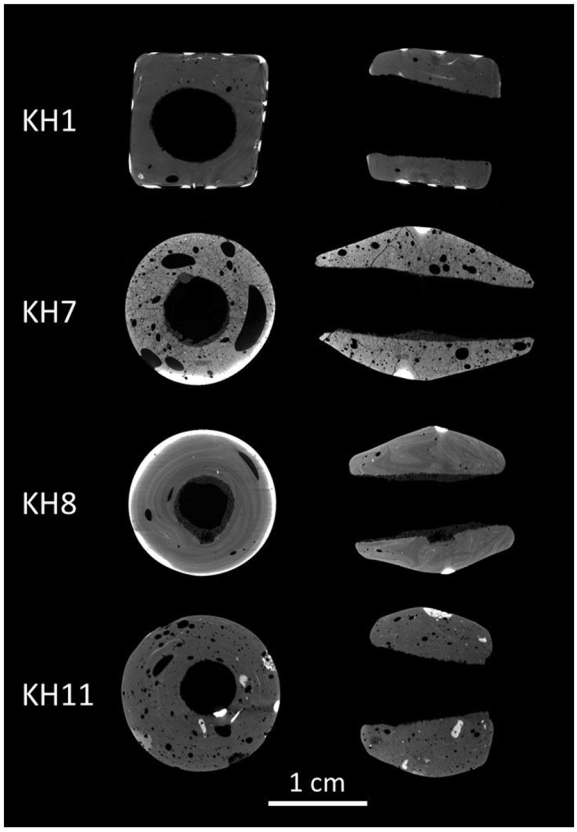

Fig. 2 Exemplary axial and longitudinal slices of the beads included in this study. Bubbles, low-Z inclusions, high-Z inclusions and decorations are visible

Discussion

Tools for bead making

All the necessary manipulations of glass at high temperature, such as making the bead, shaping it, and applying decorations, require some tools. These tools are very rarely attested in the archaeological record. In particular, at the best of the authors knowledge there is no evidence of such tools in the large area where the beads under consideration were unearthed. Nevertheless, traces of some of these tools are preserved in the beads themselves, the most obvious being that of the tool that left the hole, which in the case of wound beads is the mandrel. In addition, traces of other tools may remain on the surface if the glass was at the lower end of the glass-working temperature range during the treatment.

The mandrel

The mandrel is the thin rod that acts as the core around which the soft glass was winded. It allowed the bead-maker to expose the glass to high temperatures, therefore it was made of a material that could withstand intense heat, with metal being the most obvious candidate. The inner surface of the hole of each bead reflects the shape of the mandrel surface. Compact and strongly adhering residues were interpreted by some scholars as the use of a ceramic mandrel [30]. However, it is also reasonable to assume that this material could instead be related to the use of a release agent, such as clay, applied onto a (possibly metal) mandrel [35], similar to what is documented for modern bead making [73]. The high temperature turned the clay into ceramic and fixed it to the glass walls of the bead hole, where it can remain for centuries after the bead was removed. Such residues are also present in the beads involved in this study (Fig. 3), though their nature remains presently undetermined. The 3D models of the holes and their micro-CT profiles document this lining material, and highlight its uneven thickness, although the greatest thickness was found around half the length of the hole (Fig. 4). It ranged from about 1 mm in KH7 to about 0.2 mm for KH1; in the case of KH11, only a few remnants of this layer remained in the bead hole.

The shape of the hole was approximately a truncated cone for all the beads (Fig. 2) as a result of the use of a tapered mandrel held by the bead maker at the thicker edge, allowing easy removal of the bead towards the thinner side of the tool. The full taper angle for the mandrel can be calculated by measuring two diameters along the truncated cone and the distance between them. All these values can be obtained from both the CT volumes and the photogrammetric models. The results obtained by the two approaches are consistent and are presented in Table 3. In addition, Fig. 5 shows the full taper angles for the tools used to produce each bead, and demonstrates they were quite different one to another.

Tools for shaping and decorating the beads

By combining the effect of the surface tension of the heated glass with that of the rotation of the mandrel, the bead maker was expected to obtain round beads. Therefore, in order to obtain cubic beads, the craftsman had to use specific tools. These could be either pliers or a flat surface on which the round bead could be pressed with a spatula. Repeating the process on both sides would produce the flat surfaces of the bead.

Some bead decoration techniques also required the use of additional tools. Traces of their use can be seen on the cubic bead KH1. They are associated with the creation of a chevron pattern. Such an ornament was obtained by applying on the black squared beads several thin spiral turns of yellow glass. Immediately after the application, while both the yellow glass and the surface of the base glass were still soft, the craftsman "combed" the decoration by moving a tool across the surface of the bead in the

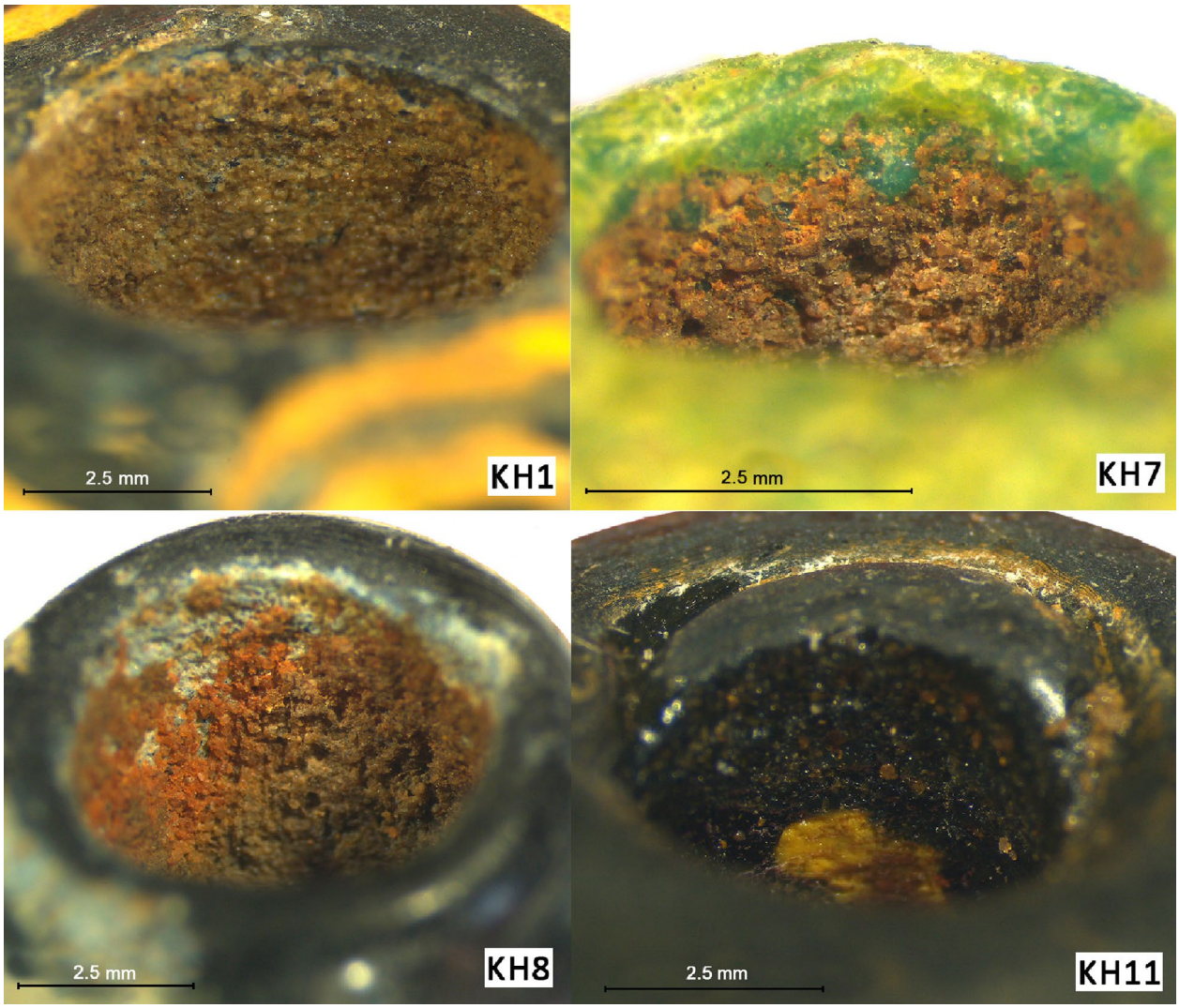

Fig. 3 Residue adhering to the inner part of the hole in the beads observed under the stereomicroscope

opposite directions, shifting the coils and creating chevrons. In some cases, the surface was soft enough to allow a flat surface to develop again, leaving no apparent trace of the combing tool. However, in other cases, short parallel furrows remained on the surface of the bead. These features are visible on several cubic beads from the burial n. 5 of the Kanfarka cemetery and, for example, on a bead from burial No. 1, mound 12 in the Perevolochan necropolis (Trans-Ural), for which a suitable photogrammetric model is available on the Sketchfab platform website (Fig. 6) [74]. This indicates that the process for making this type of bead was well-established. In the specific case of the KH1 bead, the surface of the faces is flat, with apparently no traces of the tool. However, these traces have been recorded in the CT images (Fig. 7D), where the slices clearly show grooves protruding into the base glass down to 1 mm, totally filled with the yellow glass. Due to the variable viscosity of the heated glass, these marks are irregular in shape and depth. Reconstruction of this tool is obviously difficult. However, it is reasonable to assume that the craftsman used the tip of a metal knife or a thin hook. The marks are, in fact, those of a sharp tool, because where the tool first touched the surface, the CT scans showed a deep incision (Fig. 7E). In contrast, there is less evidence of surface etching in other areas, where the action of the tool was less intense and the chevron was likely created by the soft glass being pushed towards the direction of the incision.

Tool to extract the beads from the mandrel

Some traces on KH1 can be interpreted as evidence that the beads would need to be forced out of the mandrel, despite the spacer layer. The fact that the bead was stuck on the mandrel could be related to the operations

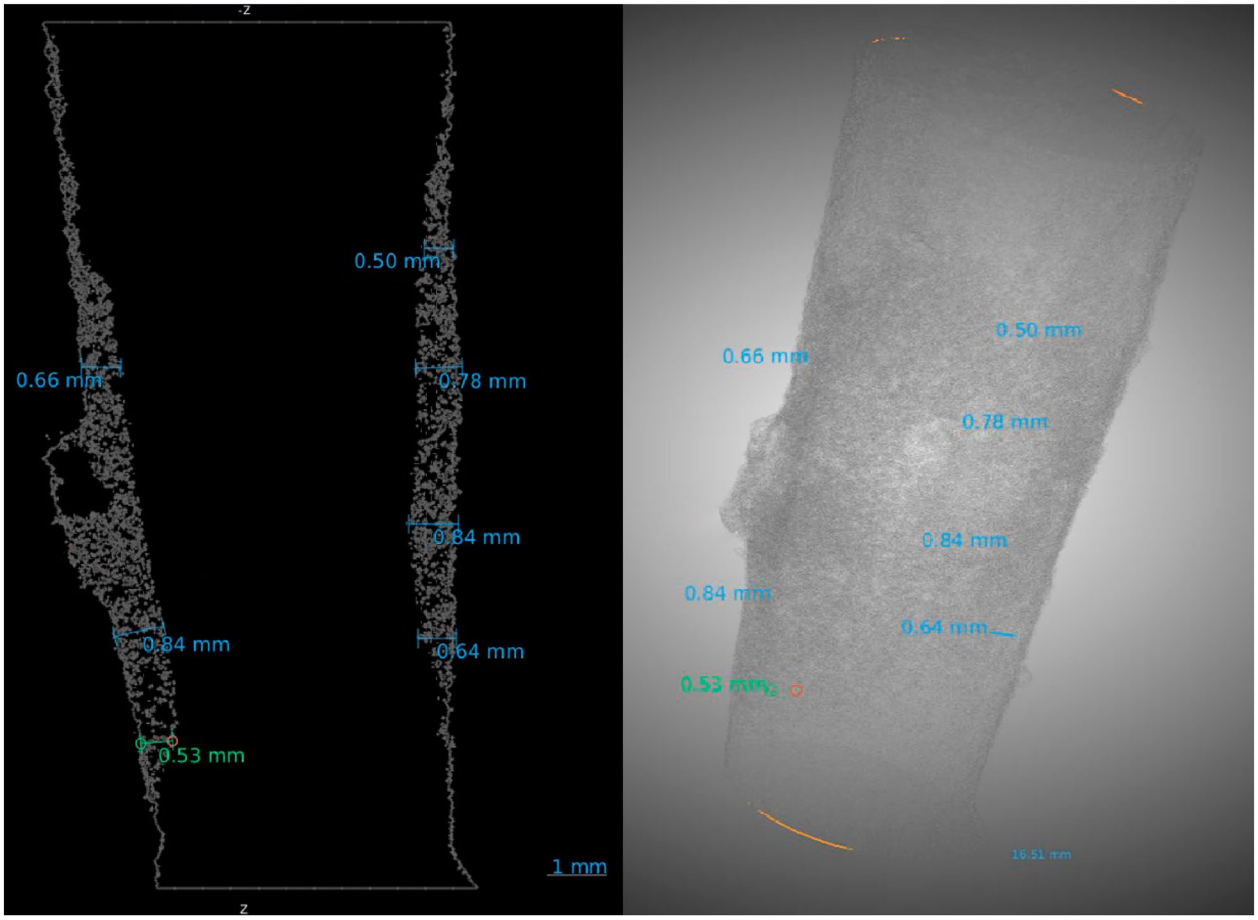

Fig. 4 The thickness of the lining material for KH 8 (micro-CT profile) and its localization on the surface of the hole (2D projection of the 3D model)

Table 3 The full taper angle for the mandrels

Lab. Id	CT (minor axis) (degrees)	CT (major axis) (degrees)	Photogrammetry (degrees)	Average (degrees)
KH1	7.2	9.4	8.3	8.3
KH7	4.6	4.8	4.0	4.5
KH8	6.1	6.6	6.3	6.3
KH11	13.5	14.7	14.1	14.1

that were performed to force the originally spherical shape into a cube. In this case, the craftsman had to press the bead from the side of the larger mandrel diameter leaving a mark on the surface, which testifies that the glass was still soft enough during the extraction of the bead. A deep mark with rounded edges is clearly seen near the side of the hole with the larger diameter (Fig. 7B). The trace left by this tool would indicate that it was not sharp, to prevent excessive deformation of the bead.

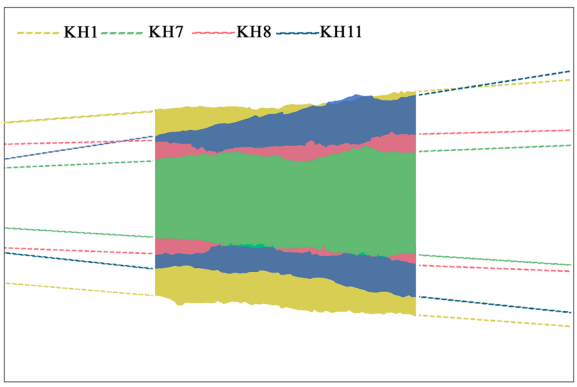

Fig. 5 Schematic view of the full taper angles for the mandrels employed in the creation of the beads considered in this work (data from Table 3)

Techniques of production

The interpretation of the features revealed by the micromorphological study of the surface and the body of the

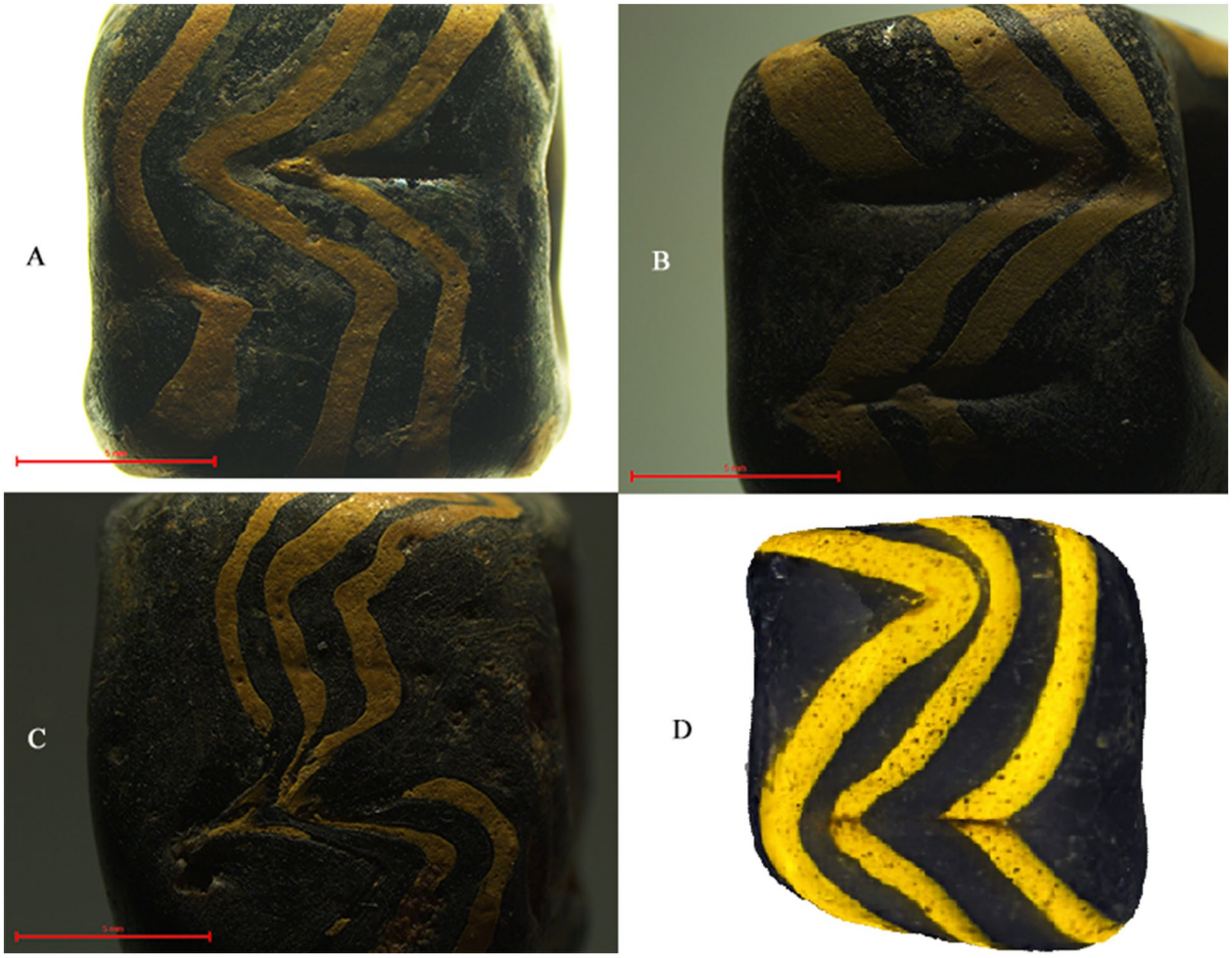

Fig. 6 Grooves left by the tool used to obtain the chevron decoration, **A**–**C** beads from the Kanfarka burial site. **D** Bead excavated from burial No. 1, mound 12, Perevolochan necropolis (data from [74])

bead allows us to reconstruct the sequence of the operations made by the bead maker.

Cubic black bead KH1

The first step in creating the KH1 cubic black bead with the yellow chevron decoration was to wind the hot black glass mass onto a mandrel. Characteristic features of the winding technique are individual elongated bubbles inside the glass bead (Fig. 7C) or traces of different radiopaque material that curl around the central hole. In addition, the rotation is evidenced by traces on the surface, which leave separate strips of glass during winding. At this stage, the shape of the bead would remain round.

The next step was to change the shape of the bead by repeatedly heating and pressing it with a plane against another plane to create the faces and edges of a cube. Remnant features of this process can be seen in the shape and orientation of the bubbles inside the body of the bead (Fig. 7D). The pre-existing bubbles moved closer to the surface of the bead and were stretched toward its corners as a result of the pressure applied by the bead maker. Additional evidence of the process of re-heating and compression of the bead surfaces is provided by a layer of seeds parallel to the faces of the cubic beads (Fig. 7F). This layer of very small bubbles was then disturbed by the tool used to create the yellow chevrons, providing information also about the decoration step (see below in this section).

Changing the shape of the bead fundamentally affected the general location and shape of the bubbles inside the bead. Repeated strong heating restored the spherical shape of some of them, the deformation changed their direction and created new ones, but some of the bubbles closest to the hole kept their original shape along the direction of the rotation. The craftsman's manipulations for the formation of the cubic shape may also change the initially conical shape of the hole, making it oval in cross section, with the longer axis of the oval being

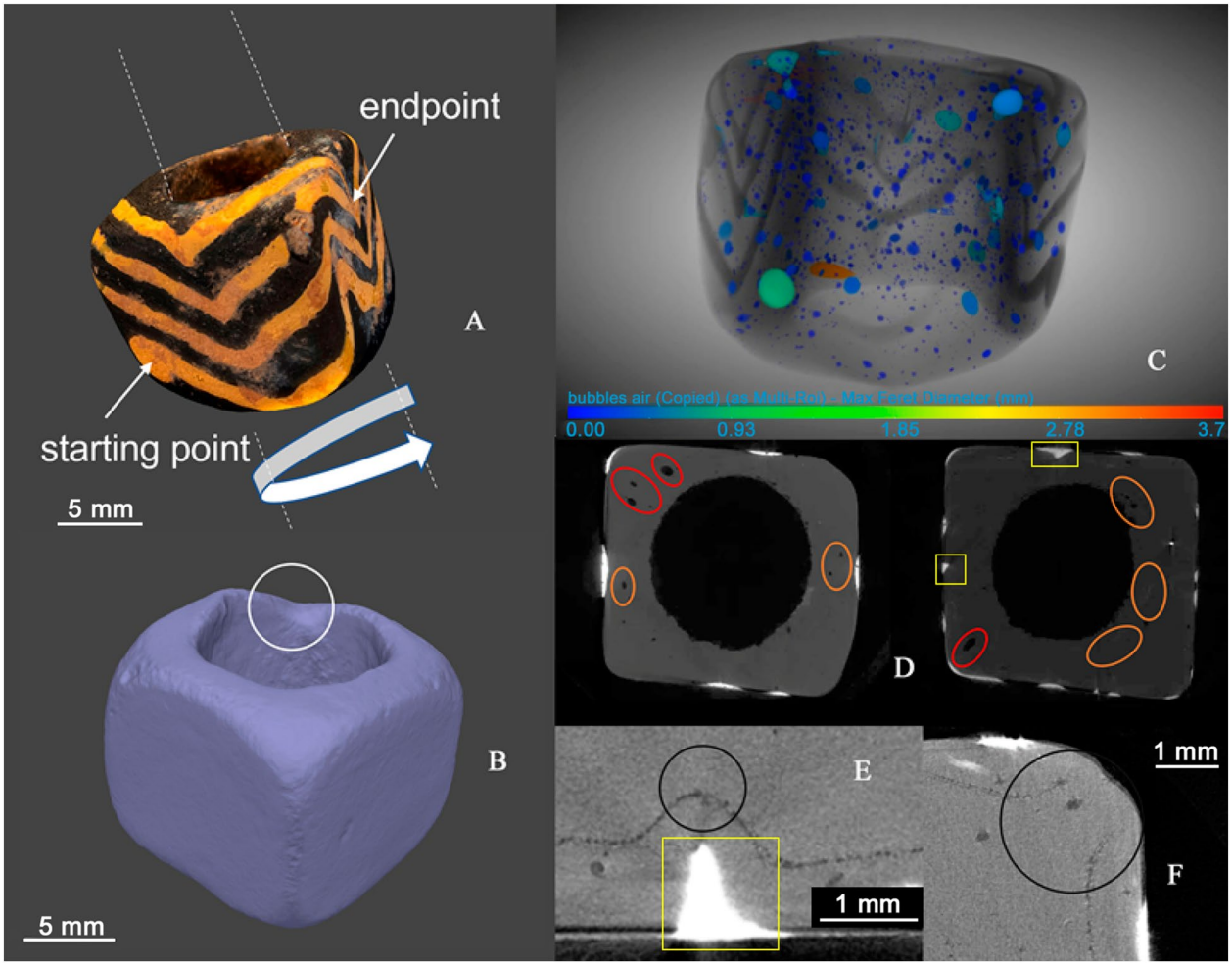

Fig. 7 Details from photogrammetry and CT scans for the bead KH1. **A** Direction of the rotation of the mandrel during bead formation and decoration. Start point and end point of the decoration are marked. **B** Surface of the bead from the photogrammetric model: the circle marks the traces left by a tool used to remove the bead from the mandrel. **C** Size distribution and shape of the bubbles in the reconstructed CT volume (colors of the bubbles depends on their size). **D** Axial CT slices highlighting peculiar directions and shapes of the bubbles also grooves protruding into the base glass (see text for details). **E** Chain of seeds (very small bubbles) created by the processes for shaping the bead into a cube and the mark of deep incision. **F** Deformation of the chain of seeds by the tool used on the edge of the cubic bead

parallel to the two faces that were pressed when the hole was deformed. This feature of the hole is visible in KH1 (Fig. 2), but this is not a general feature of the beads of the same type.

The last step was the creation of the decoration, which was done with bubbly yellow glass. 3.5 turns of the thin decorative material were applied to the bead while rotating the mandrel counterclockwise. The beginning of the application of yellow glass is marked by a large spot of excess material, the end is marked by a thin curl, with the starting point being on the larger part of the conical mandrel (Fig. 7A). Then the chevrons were created by "combing" the decorative material on the soft surface of the bead. This process caused the displacement of the soft surface layer of the black glass in opposite directions and left thin grooves on the bead surface. These grooves were noted on all the beads of the same type from the Kanfarka burial site and from the Perevolochan necropolis (Fig. 6), with the noticeable exception of the bead KH1.

In all the beads of this type from the Kanfarka cemetery, except the bead KH1, the beadmaker used the tool twice on each of the four sides of cubic bead, with two opposite movements, both parallel to the axis of the bead. In KH1, the combing tool was also used along the edges. Evidence of this treatment is highlighted by the micro-CT images (Fig. 7F). As already discussed in Sect. "Tools for shaping and decorating the beads", the tool left evident sharp indentations under the surface which, for the KH1 bead,

are filled with the yellow glass. On the faces, where the chevron was created only by the movement of the surface layer of the black glass with a tool, the CT scans recorded deformations of the layer of the seeds (Fig. 7E and F). Given that the craftsman must have deformed the edges of the bead KH1, it is difficult to explain the absence of the traces by repeated heating alone. It is therefore likely that, after the chevrons were formed, the partially deformed edges were restored by pressing the decorated bead again with the same tool used for the preliminary formation. This procedure would have been carried out only on the minority of items for which the movements of the combing tool were not precisely adjusted onto the flat surface of the bead.

A process in which the yellow decoration was placed and combed into a chevron before the bead was formed into a cube seems less convincing, as reheating is necessary to bring the originally round bead into its final cubic shape. As the decoration is high-Pb glass, it would be significantly deformed by the heating of the beads to a temperature suitable for softening the (low-Pb) base glass. This would result in irregular and thick yellow lines, possibly even wider than the gap that is left between them. Such imperfections are not common in beads of this type, although they can sometimes be seen on only one or two sides as evidence of some final shape adjustment performed by the bead maker.

Barrel shaped green bead KH7

The dense network of cracks and the sugary texture that characterize the body and the surface of the green barrel-shaped bead with a yellow linear decoration (Figs. 1, 2) may suggest that it was formed by heating crushed glass in a mold [22]. However, the elongated medium-sized bubbles curling around the central aperture, as seen in the CT scans (Fig. 2), provided sufficient evidence for the winding technique. For this bead, the poor state of preservation may prevent the detection of features that suggest any technical details. Nonetheless, a series of thin bubbles forming characteristic curls was noticeable, and can be read as an indication of clockwise rotation of the mandrel, with the bead developing as a spiral in the direction opposite to the position of the hand holding the mandrel (Fig. 8B).

The swirls that formed the bulk of the bead were superimposed on the mandrel with an angle of approximately 75°. The traces of rotation are visible on the surface of the bead itself and are expressed as alternating light green and dark green stripes (Fig. 8A). The lighter-coloured green glass does not feature any non-glassy inclusion, as evident from the CT scan. So, its colour is not augmented by the presence of the opacifier. By carefully observing the surface texture of the bead in the photogrammetric model, it became clear that the light green color could be due to the development of a much larger number of surface cracks (Fig. 1). This degradation of the bead does not appear to correlate with the location of the cracks within the glass itself or with materials with different composition (that would show different radiopacity). It is most likely that this effect has occurred over time due to uneven internal stress of the glass caused by insufficient annealing. These irregularities may also be the cause of the large bubbles that, in some cases, have reached the surface, creating deep cavities and making the object even more fragile. Combination of CT scans and photogrammetry proved to be promising strategy for conservation state characterisation.

Once the bulk of the bead was formed, it was decorated with a thin yellow ring around the largest circumference. The glass of the decoration features numerous cracks, but in a different pattern than the green base glass. The junction (where the start and the end overlap) of the decorative ring is not visible on the surface. Voxels of the decorative ring were extracted from the rest of the volume and presented in Fig. 8D. The zoomed up section of the ring in the marked place (cross-section 1 in Fig. 8D) is thicker than in the rest of the ring (cross-section 2 in Fig. 8D) and demonstrates certain fold of the glass, marked in the figure. This thicker spot is assumed to be the junction. According to these images, the direction of rotation of the bead during the application of the decoration was clockwise, which corresponds to the direction of the rotation during the creation of the green core. The CT volumes also highlighted the thin bubbles in the yellow glass which, thanks to the heat, did not show any stretching in the direction of the rotation and appeared spherical.

Barrel shaped black bead KH8

The most striking feature of bead KH8 is the uneven composition of the glass, which is reflected in slightly different textures on the bead surface, documented in the photogrammetric models and in patterns of differently radiopaque materials within the body of the bead, tracing the direction and sequence of the wound glass (Fig. 9C). This may be related to the technique of using individually gathered chunks of softened glass to wind the glass around the mandrel, a procedure that was common throughout the Bronze Age until the first century BCE [22].

To make the bead, the craftsman rotated the mandrel clockwise, applying turns of the glass one after the other, going forward in the opposite direction from the position of the hand holding the mandrel. At least six of such turns are visible, ending with a thin curl visible on the surface of the bead (Fig. 9A). The glass was

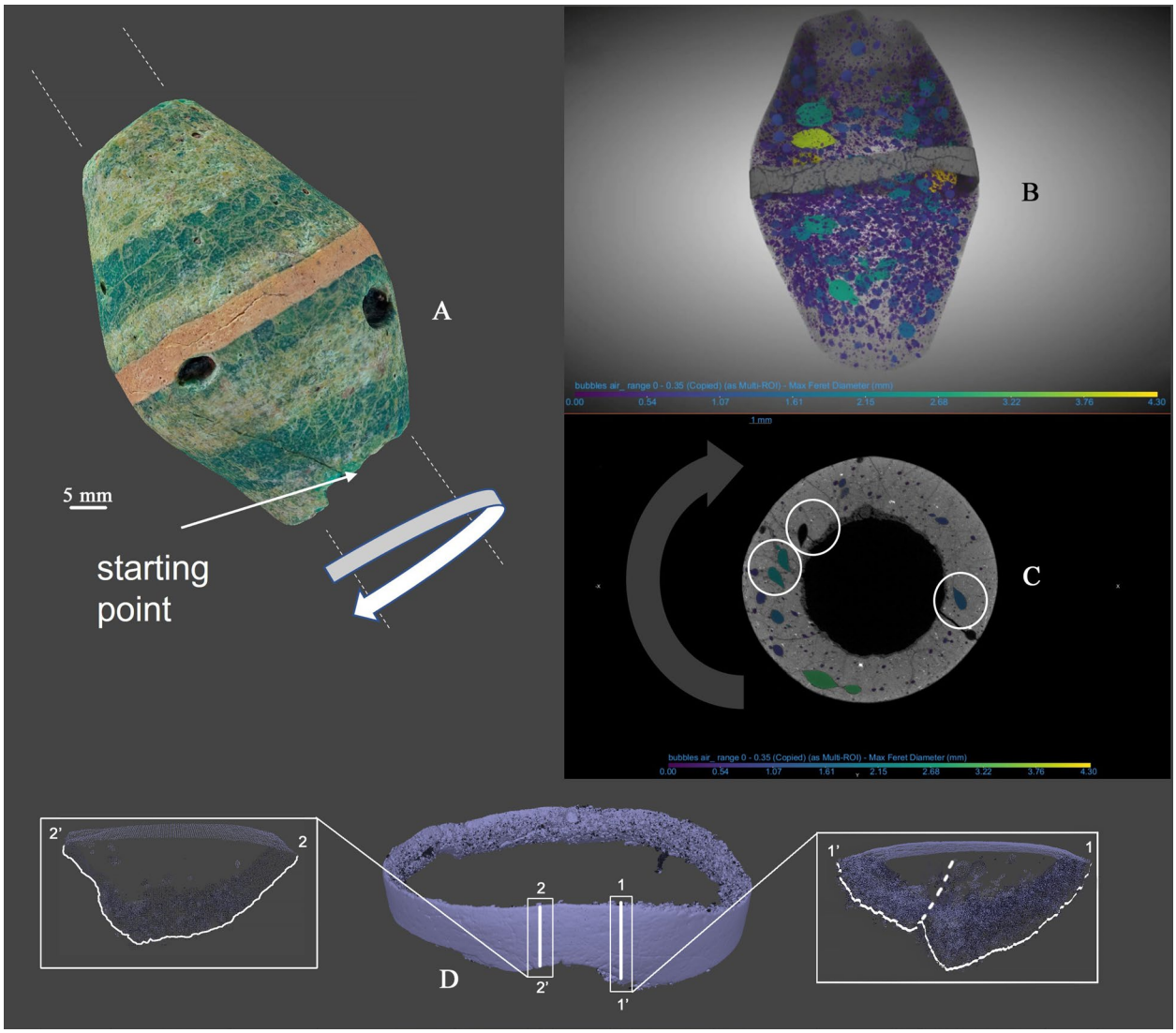

Fig. 8 Details from photogrammetry and CT scans for the bead KH7. **A** Direction of the rotation of the mandrel during the bead formation and decoration. The starting point for the bead formation is indicated. **B** Size distribution and shape of the bubbles in the reconstructed CT volume (colour of the bubbles depends on their size). **C** Axial CT slices highlighting peculiar directions and shapes of the bubbles (see text for details). **D** CT representation of the decoration with cross-sections: 1—overlapping of the start/finish point; 2—typical cross section of the rest of the decoration

applied to the mandrel at an angle of 81–85°, and the direction of the rotation can be easily reconstructed from the surface features that are visible in the photogrammetric 3D model (Fig. 9A). This conclusion is also corroborated by the shape of the bubbles in the micro-CT volume (Fig. 9D). The largest of them are elongated around the bore, with the same angle as the glass with respect to the axis of the mandrel. Some of the larger bubbles are unevenly stretched, featuring what we can conventionally call a "head" and a "tail" (Fig. 9B and D). In this case, the head indicates the direction of the rotation of the bead. The most likely explanation for the appearance of such bubbles is the entrapping of gasses between the individual turns of the glass mass as they overlap. The smallest bubbles are spherical and do not give hints about rotation. Very small non-glassy inclusions aligned in the direction of winding can be observed in the 3D model constructed from CT slices (Fig. 9F). On the surface of the bead (using photogrammetric 3D model) in the same places it is possible to see certain lines going in the same direction. By combining the two 3D models it is therefore possible to compare traces of production that appear both inside the bead and on its surface.

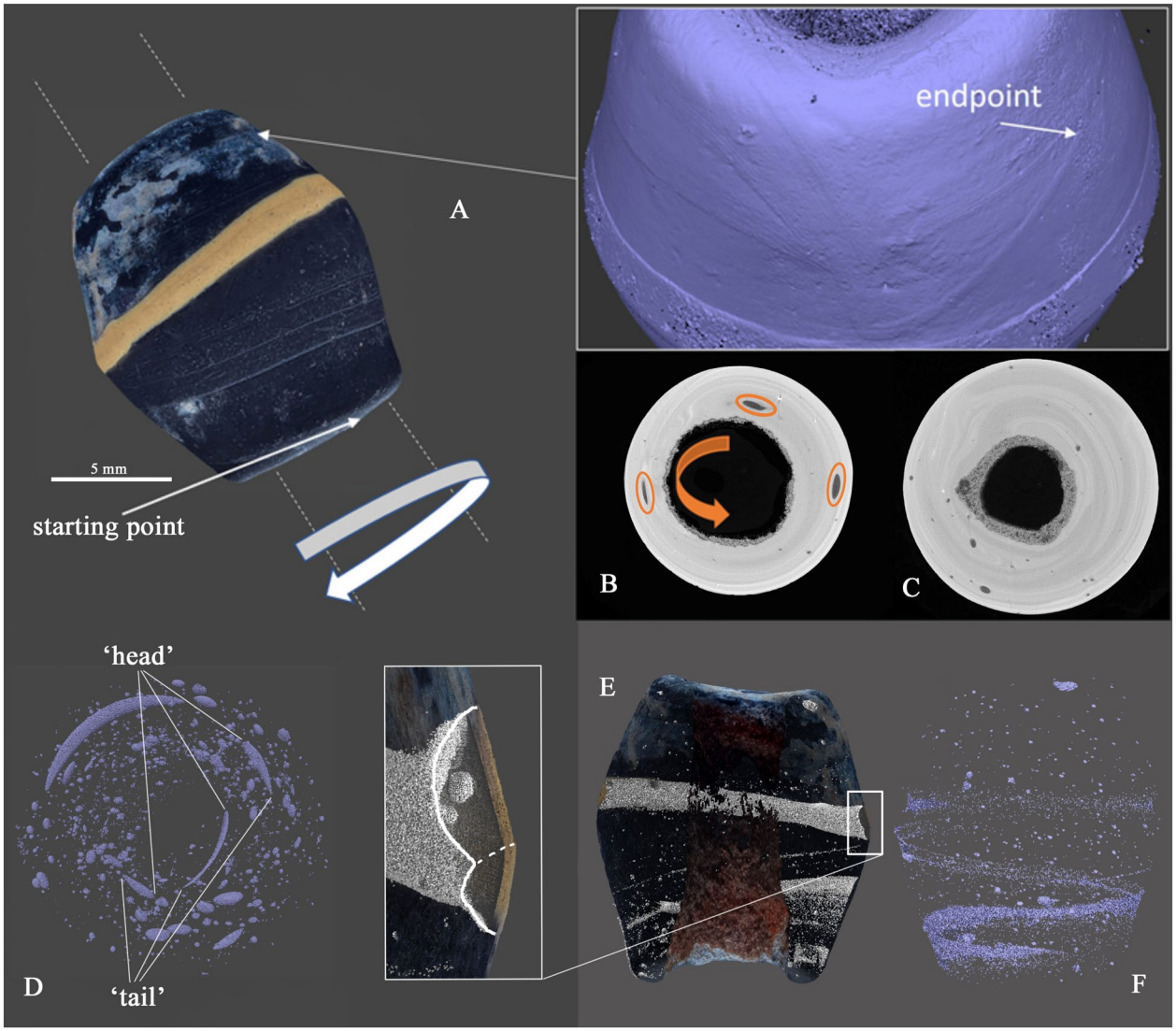

Fig. 9 Details from photogrammetry and CT scans for the bead KH8. **A** Direction of the rotation of the mandrel during bead formation and decoration. The starting point and ending point for the bead formation are indicated. **B** Elongated bubbles marking the direction of the rotation of the mandrel during the bead making, **C** Axial CT slice highlighting the layers of different glass. **D** Shape of the bubbles obtained by segmenting the CT volume. Several examples of "head and tail" bubbles are highlighted. **E** 3D model resulting from the combination of photogrammetric and micro-CT data. The detail of the junction of the ring decoration is also shown, **F** distribution of high-density inclusions (except the ring decoration) demonstrating the winding pattern

Similarly, the rotation and overlapping of the glass layers are visible in the micro-CT images of the transverse planes. The increase of thickness in the central part of the bead was achieved by applying an additional layer of glass.

After creating the core of the bead, the bead maker added a simple decoration by applying a thin stripe of yellow glass near the largest circumference of the bead, perpendicular to its axis. The joint in the starting/finishing point of the decoration is uneven and is visible on the surface. In addition, thanks to the profile of the decorative stripe that was obtained by segmenting the CT volume, it is possible to distinguish its beginning and the end (Fig. 9E). This allows us to reconstruct the direction of rotation of the bead during the creation of the decoration and it corresponds to the direction of its rotation during the forming of the bulk. The yellow glass features a much higher porosity than the base glass, and is covered with numerous superficial cracks. Numerous spherical bubbles can also be seen inside the decoration thanks to the CT reconstructed volume (Fig. 9E).

Round black bead with colored spots KH11

The black rounded bead with uneven colored spots KH11, like the other beads considered in this work, shows features that indicate the winding technique. Traces on the surface of the bead allowed to identify the point where the first glass was deposited on the mandrel, which was then rotated clockwise (Fig. 10A). The coils of glass mass were applied in the direction of the taper, meaning towards the opposite direction to the bead maker's hand. The oblate bubbles, stretched perpendicularly to the aperture of the bead, are recorded in large numbers (Fig. 10B and D). In this case, the bead surface does not show any traces of the glass coils applied by the artisan to form the bead. However, micro-CT profiles revealed a thin spiral of more radiopaque material twisting outwards from the aperture, which suggests that the bead body was formed by at least three layers of glass (Fig. 10C).

After the bead was formed, the bead maker applied the decorations that are now visible on the surface as yellow, red, and white uneven spots. These are concentrated along the largest diameter of the bead, while they

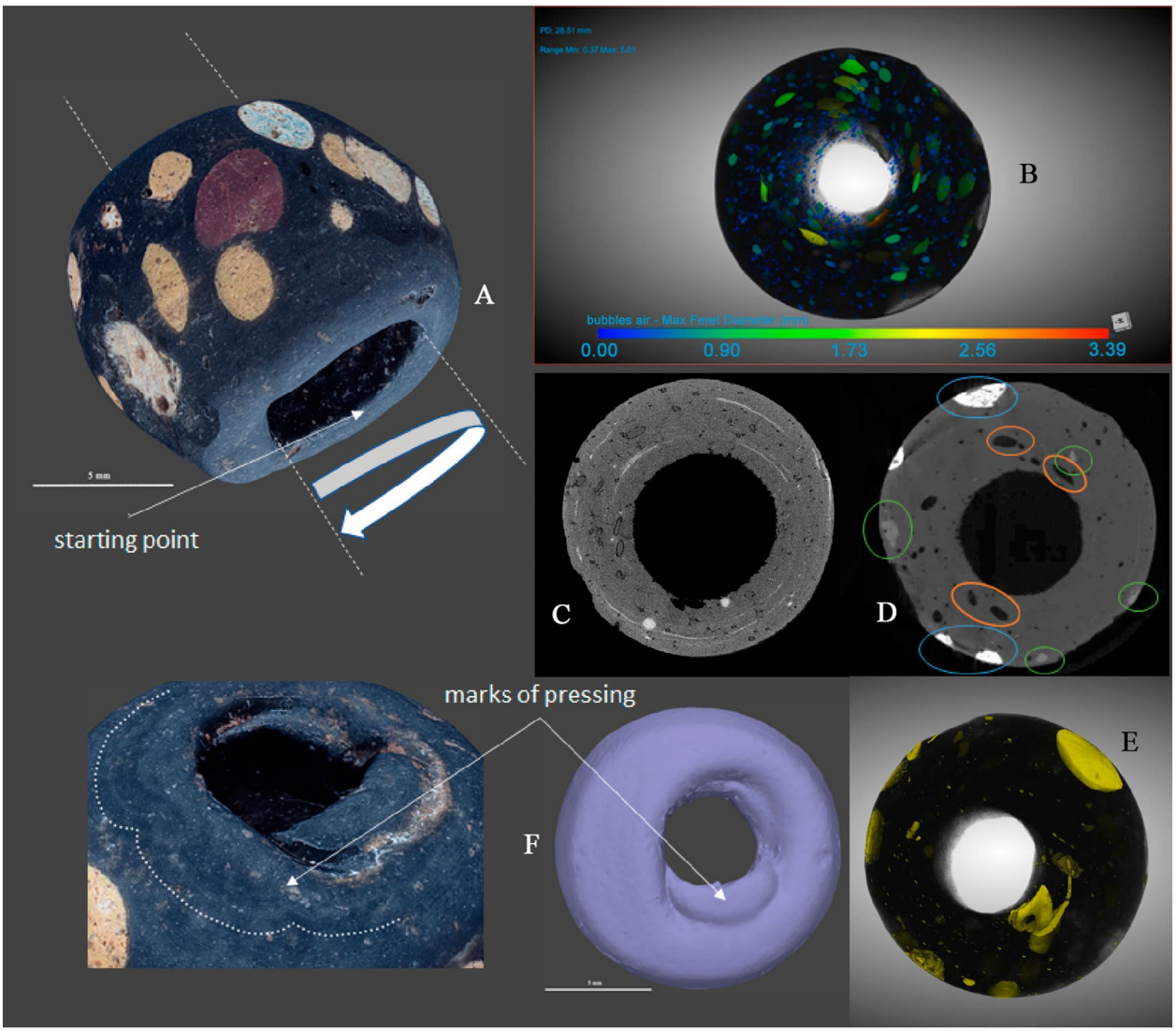

Fig. 10 Details from photogrammetry and CT scans for the bead KH11. **A** Direction of the rotation of the mandrel during the bead formation. The starting point of the formation is marked. **B** Size distribution and shape of the bubbles in the reconstructed CT volume (colors of the bubbles depends on their size). **C** Axial CT slice highlighting a thin spiral of radiopaque material twisting outwards from the aperture. **D** Axial CT slice highlighting decorations (marked with blue ellipses), medium-Z inclusions (green) and oblate bubbles (orange). **E** High-Z material sunken in the base glass. **F** Details of the flattened area near the aperture, showing traces of a post treatment to refine the apex of the bead

are absent from the flattened areas near the apertures. CT scans revealed that the spots protrude with rounded edges into the dark base glass, where medium-Z inclusions are also visible (Fig. 10D); moreover, some highly radiopaque material in the bulk of the bead below the surface was also detected (Fig. 10E).

Again, the glass used for the decoration features a large number of round bubbles. It is reasonable to assume that the bead maker may have used a special decoration technique in which the heated bead is rolled onto a flat surface on which chips of colored glass were scattered [75]. The soft surface would allow them to be embedded, and additional heating/marvering would also support the development of a flat surface, in which the glass of the decoration does not extend above that of the dark glass.

On the side of the smaller aperture diameter, this bead features specific traces that would suggest the presence of glass that extended beyond the apex, which was then softened and pressed into the bead (Fig. 10F).

Such a trace of additional glass is documented in the archaeological record as an indication that many beads were made on the same mandrel, with a thin thread connecting them all. This thin glass was then broken by the bead maker after all the manipulations were completed [35]. The shape of the bead suggests that the bead was then pressed on a hot flat surface to allow the excess glass to soften and to sink into the apex of the bead, which in turn was flattened.

Further evidence of this treatment is the scalloped pattern visible on the surface around the aperture (Fig. 10F), which may have resulted from the contact with a hot surface. Such a treatment would also explain the characteristic texture found on the surface of this bead (Fig. 1D1–D3), with dense wrinkles running perpendicularly to the aperture, although we cannot exclude that this feature could also be related to marvering.

Conclusions

The bead making process leaves some physical traces in the glass, and these traces can be revealed by a thorough examination of the finished object. For archaeological glass beads, the examination can be carried out by magnifying the surface under an optical or electron microscope, revealing the features that would guide the interpretation of the technology behind the bead, or by examining both the photogrammetric 3D models and the CT reconstructed volumes, which provided a much deeper level of insight.

This approach proved to be very useful in reconstructing the bead making processes, as both micro-CT and photogrammetry were able to document and accurately measure some elements from the surface and below, in many cases providing complementary data.

The (virtual) objects were fully explored, and various combinations of the point clouds obtained from the two 3D imaging techniques provided new perspective that helped to pinpoint features relevant to reconstruct the bead making technique.

All the data collected within this study corroborate the established knowledge of the bead making techniques of the period and present a framework for their analysis that includes a comprehensive view provided by several methods.

We established that all four beads were made by winding hot glass around a mandrel. One of the most prominent outcomes of this research is the approach for tracking the direction of the mandrel rotation during the different steps of the bead production. For most of the beads the mandrel was rotated clockwise during the formation of the bead. For the cubic bead, which underwent deep manipulation to be shaped as a cube, it was not possible to recognize the direction of mandrel rotation, but the decoration was obtained by rotating the mandrel counterclockwise. In all the operations involving rotation, the starting point of the operation went forward in the opposite direction with respect to the hand holding the mandrel.

Although the rotation of the mandrel is not systematically investigated in previous studies, and there are currently no significant comparative data, we believe that it will be considered in the future to gain further insight into the technology of past cultures, taking advantage of the opportunities offered by 3D imaging methods to provide information on this intangible aspect of bead making.

This work demonstrates the merit of combining photogrammetry and micro-CT beyond the already popular application for 3D digitization for archival recording and provides an unprecedented insight into the micromorphology of several types of fourth century BCE glass beads found in a vast area of Eastern Europe, enriching the limited set of data already available for archaeological glass beads.

Abbreviations

BCE	Before common era
CMOS	Complementary metal-oxide-semiconductor
CT	Computed tomography
INFN	Instituto nazionale di fisica nucleare (italian national institute for nuclear physics)
SEM–EDS	Scanning electron microscopy—energy dispersive microscopy

Supplementary Information

The online version contains supplementary material available at https://doi.org/10.1186/s40494-023-01078-0.

Additional file 1: Figure S1. Images of the beads from an archival documentation perspective.

Acknowledgements
Authors would like to express their gratitude to the administration of Khortytsia National Reserve (Zaporizhzhia, Ukraine) for providing materials for the analysis.

Author contributions
DN: conceptualization, validation, formal analysis, investigation, methodology, writing-original draft, visualization, data curation; OY: investigation, visualization, validation, writing—review and editing; LG: formal analysis, writing-original draft, writing—review and editing; ALG: methodology, formal analysis, resources, funding acquisition, supervision; FT: methodology, formal analysis, validation, data curation, writing—review and editing; LPC: methodology, formal analysis, validation, data curation, writing—review and editing; GS: formal analysis, validation, data curation, funding acquisition; PD: formal analysis, validation, data curation; MG: conceptualization, validation, investigation, methodology, writing-original draft, writing—review and editing, supervision, funding acquisition; AR: conceptualization, validation, methodology, writing—review and editing, supervision. All authors read and approved the final manuscript.

Funding
DN`s work has been supported by a special grant from the University of Torino as part of the "Support initiative for Ukrainian scholars—Azioni di supporto a favore di studiosi e studiose ucraini/e". This project has received funding from the European Union's Horizon 2020 research and innovation program under the Marie Skłodowska-Curie grant agreement No 754511. The contents of this paper are the sole responsibility of the authors and do not necessarily reflect the opinion of the European Union.

Availability of data and materials
Data that are not explicitly presented in the paper or the Additional file may be provided on a reasonable request by the corresponding author. The photogrammetric 3D models used in the paper are available on the sketchfab.com repository (https://sketchfab.com/dnykonen/models).

Declarations

Ethics approval and consent to participate
Not Applicable.

Consent for publication
Not applicable.

Competing interests
The authors declare that they have no competing interests.

Received: 7 August 2023 Accepted: 26 October 2023
Published online: 13 November 2023

References

1. Bandama F, Chirikure S, Hall S, Tinguely C. Measly but motley and manifest: the typological and chemical characterisations of glass beads from the Southern Waterberg, Limpopo province of South Africa. J Archaeol Sci Rep. 2018;18:90–9. http://doi.org/10.1016/j.jasrep.2017.12.047.
2. Boschetti C, Gratuze B, Schibille N. Commercial and social significance of glass beads in migration-period Italy: the cemetery of Campo Marchione. Oxf J Archaeol. 2020;39:319–42. http://doi.org/10.1111/ojoa.12200.
3. Cheng Q, Zhang X, Guo J, Wang B, Lei Y, Zhou G, et al. Application of computed tomography in the analysis of glass beads unearthed in Shanpula cemetery (Khotan), Xinjiang Uyghur autonomous region. Archaeol Anthropol Sci. 2019;11:937–45. http://doi.org/10.1007/s12520-017-0582-6.
4. Fitzgerald WR, Knight DH, Bain A. Untanglers of matters temporal and cultural: glass beads and the early contact period huron ball site. Can J Archaeol. 1995;19:117–38.
5. Ngan-Tillard DJM, Huisman DJ, Corbella F, Van Nass A. Over the rainbow? Micro-CT scanning to non-destructively study Roman and early medieval glass bead manufacture. J Archaeol Sci. 2018;98:7–21. http://doi.org/10.1016/j.jas.2018.07.007.
6. Truffa Giachet M, Gratuze B, Mayor A, Huysecom E. Compositional and provenance study of glass beads from archaeological sites in Mali and Senegal at the time of the first Sahelian states. PLoS ONE. 2020;15:e0242027. http://doi.org/10.1371/journal.pone.0242027.
7. Beck HC. Classification and nomenclature of beads and pendants. Archaeologia. 1928;77:1–76. http://doi.org/10.1017/S0261340900013345.
8. Karklins K. Guide to the description and classification of glass beads found in the Americas. BEADS J Soc Bead Res. 2012;24:62–90.
9. Kidd KE, Kidd MA. A Classification System for Glass Beads for the Use of Field Archaeologists. BEADS J Soc Bead Res. 2012;24:39–61.
10. Pion C. Les perles mérovingiennes: typo-chronologie, fabrication et fonctions [Thèse de doctorat]. [Bruxelles]: Université libre de Bruxelles; 2014.
11. Dekówna M, Olczak J. Principes de description des verres ancien depuis les temps les plus reculés jusq'au XIIIe siécle de n.é. Wydawnictwo DiG. Warszawa–Toruń; 2002.
12. Maltoni S, Chinni T, Vandini M, Cirelli E, Silvestri A, Molin G. Archaeological and archaeometric study of the glass finds from the ancient harbour of Classe (Ravenna- Italy): new evidence. Herit Sci. 2015;3:13. http://doi.org/10.1186/s40494-015-0034-5
13. Rehren Th, Freestone IC. Ancient glass: from kaleidoscope to crystal ball. J Archaeol Sci. 2015;56:233–41. http://doi.org/10.1016/j.jas.2015.02.021
14. Costa M, Barrulas P, Dias L, da Conceição LM, Barreira J, Clist B, et al. Multi-analytical approach to the study of the European glass beads found in the tombs of Kulumbimbi (Mbanza Kongo, Angola). Microchem J. 2019;149:103990. http://doi.org/10.1016/j.microc.2019.103990.
15. Degryse P, Scott RB, Brems D. The archaeometry of ancient glassmaking: reconstructing ancient technology and the trade of raw materials. Perspective. 2014. https://doi.org/10.4000/perspective.5617.
16. Freestone IC. The Provenance of Ancient Glass through Compositional Analysis. MRS Proc. 2004;852:OO8.1. https://doi.org/10.1557/PROC-852-OO8.1
17. Schibille N, Marii F, Rehren Th. Characterization and provenance of late antique window glass from the Petra church in Jordan*. Archaeometry. 2008;50:627–42. http://doi.org/10.1111/j.1475-4754.2007.00346.x
18. Saminpanya S, Saiyasombat C, Thammajak N, Samrong C, Footrakul S, Potisuppaiboon N, et al. Shedding new light on ancient glass beads by synchrotron, SEM-EDS, and Raman spectroscopy techniques. Sci Rep. 2019;9:16069. http://doi.org/10.1038/s41598-019-52322-2
19. Yang Y, Wang L, Wei S, Song G, Kenoyer JM, Xiao T, et al. Nondestructive analysis of dragonfly eye beads from the Warring States period, excavated from a Chu Tomb at the Shenmingpu Site, Henan province. China Microsc Microanal. 2013;19:335–43. http://doi.org/10.1017/S1431927612014201
20. Tamura T, Oga K. Archaeometrical investigation of natron glass excavated in Japan. Microchem J. 2016;126:7–17. http://doi.org/10.1016/j.microc.2015.11.029
21. Then-Obłuska J. Typology of Glass Beads: Techniques, Shapes, Colours and Dimensions. In: Kanungo AK, Dussubieux L, editors. Ancient Glass of South Asia. Singapore: Springer Singapore; 2021. p. 211–24. https://doi.org/10.1007/978-981-16-3656-1_8.
22. Bertini M, Mokso R, Krupp EM. Unwinding the spiral: discovering the manufacturing method of Iron Age Scottish glass beads. J Archaeol Sci. 2014;43:256–66. http://doi.org/10.1016/j.jas.2014.01.001.
23. Purowski T. Identifying Bronze Age glass production centres through bead-making techniques. APOL. 2023;67:61–80. http://doi.org/10.23858/APol67.2022.003.
24. Zhang X, Lei Y, Cheng Q, Zhou G. Application of computed tomography in the analysis of the manufacture of eye beads technique. Microchem J. 2020;156: 104798. http://doi.org/10.1016/j.microc.2020.104798.
25. Sprague R, Bowers AW. Glass trade beads: a progress report. Hist Arch. 1985;19:87–105. http://doi.org/10.1007/BF03373477.
26. Neri E, Gratuze B, Schibille N. The trade of glass beads in early medieval Illyricum: towards an Islamic monopoly. Archaeol Anthropol Sci. 2019;11:1107–22. http://doi.org/10.1007/s12520-017-0583-5
27. Dussubieux L, Walder H. The elemental analysis of glass beads: technology chronology and exchange. Univ Pers Leuven. 2022. https://doi.org/10.2307/j.ctv2z9fzr0.

28. Ostapenko MA. Scythian moundless burial grounds of the Steppe Dnipro catchment (Skifskie beskurgannye mogil'niki stepnogo Podneprov'ja). Antichnyj mir i varvary na juge Rossii i Ukrainy Ol'vija Skifija Bospor. Dyke pole. Zaporizhzhia; 2007. p. 143–79.
29. Ostapenko MA. Non-nomadic population sites of the Scythian time on the Khortytsia island. (Pamiatky osilosti skifskoho chasu na ostrovi Khortytsia). Arkheolohiia. 2001;1:51–67.
30. Alexeeva EM. Antique beads of North Black Sea region. Antichnye busy Severnogo Prichernomor'ja. Nauka. Moskow; 1978.
31. Terenozhkin AI, Ilyinskaya VA, Chernenko IV, Mozolevsky BN. Scythian mounds of Nikopol area. (Skifskie kurgany nikopol'shhiny). Skifskie drevnosti. Naukova dumka. Kyiv; 1973. p. 113–86.
32. Liberov PD. Sites of the Scythian time in the Middle Don river catchment. (Pamjatniki Skifskogo vremeni na Srednem Donu). Nauka. Moscow; 1965.
33. Anikeeva OV. Appearing and origin of the sets of beads from burial 5 mound 3 Kichigino I site in south Ural region. (Proishozhdenie i Vremja Pojavlenija na Juzhnom Urale Bus iz naborov Pogrebenija 5 Kurgana 3 Mogil'nika Kichigino I). Chelyabinsk: Gosudarstvennyj istoricheskij muzej Juzhnogo Urala; 2017. p. 14–23.
34. Klepikov VM, Skripkin AC. Chronology of the early Sarmatian sites of the lower Volga catchment. (Hronologiia Rannesarmatskih Pamjatnikov Nizhniego Povolzh'ja). Nizhnevolzhskij Arheologichskij Vestnik. 2002;47–81.
35. Alexeeva EM. Antique beads of North Black Sea region. Moscow: Antichnye busy Severnogo Prichernomor'ja. Nauka; 1975.
36. Hughes S. CT Scanning in Archaeology. In: Saba L, editor. Computed Tomography—Special Applications. InTech; 2011. http://www.intechopen.com/books/computed-tomography-special-applications/ct-scanning-in-archaeology. Accessed 6 Aug 2023. http://doi.org/10.5772/22741
37. Zwanenburg EA, Williams MA, Warnett JM. Review of high-speed imaging with lab-based x-ray computed tomography. Meas Sci Technol. 2022;33:012003. http://doi.org/10.1088/1361-6501/ac354a.
38. Jackowski C, Bolliger S, Thali MJ. Common and unexpected findings in mummies from ancient Egypt and South America as revealed by CT. Radiographics. 2008;28:1477–92. http://doi.org/10.1148/rg.285075112.
39. McKnight LM, Atherton-Woolham SD, Adams JE. Imaging of ancient Egyptian animal mummies. Radiographics. 2015;35:2108–20. http://doi.org/10.1148/rg.2015140309.
40. Nava A, Coppa A, Coppola D, Mancini L, Dreossi D, Zanini F, et al. Virtual histological assessment of the prenatal life history and age at death of the upper paleolithic fetus from Ostuni (Italy). Sci Rep. 2017;7:9427. http://doi.org/10.1038/s41598-017-09773-2.
41. Re A, Corsi J, Demmelbauer M, Martini M, Mila G, Ricci C. X-ray tomography of a soil block: a useful tool for the restoration of archaeological finds. Herit Sci. 2015;3:4. http://doi.org/10.1186/s40494-015-0033-6.
42. Gait J, Bajnok K, Szilágyi V, Szenti I, Kukovecz Á, Kis Z. Quantitative 3D orientation analysis of particles and voids to differentiate hand-built pottery forming techniques using X-ray microtomography and neutron tomography. Archaeol Anthropol Sci. 2022;14:223. http://doi.org/10.1007/s12520-022-01688-y.
43. Spataro M, Taylor J, O'Flynn D. A technological study of Assyrian clay tablets from Nineveh, Tell Halaf and Nimrud: a pilot case study. Archaeol Anthropol Sci. 2023;15:68. http://doi.org/10.1007/s12520-023-01761-0.
44. Nguyen H-Y, Keating S, Bevan G, Gabov A, Daymond M, Schillinger B, et al. Seeing through Corrosion: Using Micro-focus X-ray Computed Tomography and Neutron Computed Tomography to Digitally "Clean" Ancient Bronze Coins. MRS Proc. 2011;1319:mrsf10–1319-ww03–05. http://doi.org/10.1557/opl.2011.799.
45. Dumont L, Dupuy V, Nicolas T, Pelé-Meziani C, De Mulder G. The protohistoric sword from Le Gué-de-Velluire (Vendée, France): a pasticcio's history unveiled by archaeometrical research. J Archaeol Sci Rep. 2020;34:102645. http://doi.org/10.1016/j.jasrep.2020.102645
46. Re A, Giudice AL, Nervo M, Buscaglia P, Luciani P, Borla M, et al. The importance of tomography studying wooden artefacts: a comparison with radiography in the case of a coffin lid from ancient Egypt. Int J Conserv Sci. 2016; 935–44.
47. Sodini N, Dreossi D, Giordano A, Kaiser J, Zanini F, Zikmund T. Comparison of different experimental approaches in the tomographic analysis of ancient violins. J Cult Herit. 2017;27:S88-92. http://doi.org/10.1016/j.culher.2017.02.013.
48. Tansella F, Vigorelli L, Ricchiardi G, Re A, Bonizzoni L, Grassini S, et al. X-ray computed tomography analysis of historical woodwind instruments of the late eighteenth century. J Imaging. 2022;8:260. http://doi.org/10.3390/jimaging8100260.
49. Alarashi H, Benz M, Gresky J, Burkhardt A, Fischer A, Gourichon L, et al. Threads of memory: Reviving the ornament of a dead child at the Neolithic village of Ba`ja (Jordan). PLoS ONE. 2023;18:e0288075. http://doi.org/10.1371/journal.pone.0288075.
50. Bernardini F, Vaccari L, Zanini F, Bassetti M, Degasperi N, Rottoli M, et al. Production and use of birch bark tar at the Neolithic pile-dwelling of Palù di Livenza (North-Eastern Italy) revealed by X-ray computed micro-tomography and synchrotron Fourier-transform infrared spectroscopy. Archaeometry. 2023;65:897–907. http://doi.org/10.1111/arcm.12847
51. Albertin F, Bettuzzi M, Brancaccio R, Morigi MP, Casali F. X-Ray computed tomography In Situ: an opportunity for museums and restoration laboratories. Heritage. 2019;2:2028–38. http://doi.org/10.3390/heritage2030122
52. Oliveira R, De Paula A, Gonçalves F, Bueno R, Calgam T, Azeredo S, et al. Development and characterization of a portable CT system for wooden sculptures analysis. Radiat Phys Chem. 2022;200: 110409. http://doi.org/10.1016/j.radphyschem.2022.110409
53. Re A, Albertin F, Avataneo C, Brancaccio R, Corsi J, Cotto G, et al. X-ray tomography of large wooden artworks: the case study of "Doppio corpo" by Pietro Piffetti. Herit sci. 2014;2:19. http://doi.org/10.1186/s40494-014-0019-9.
54. Bossema FG, Domínguez-Delmás M, Palenstijn WJ, Kostenko A, Dorscheid J, Coban SB, et al. A novel method for dendrochronology of large historical wooden objects using line trajectory X-ray tomography. Sci Rep. 2021;11:11024. http://doi.org/10.1038/s41598-021-90135-4.
55. Kiss MB, Bossema FG, Van Laar PJC, Meijer S, Lucka F, Van Leeuwen T, et al. Beam filtration for object-tailored X-ray CT of multi-material cultural heritage objects. Herit Sci. 2023;11:130. http://doi.org/10.1186/s40494-023-00970-z.
56. Pelt D, Batenburg K, Sethian J. Improving tomographic reconstruction from limited data using mixed-scale dense convolutional neural networks. J Imaging. 2018;4:128. http://doi.org/10.3390/jimaging4110128.
57. Lifton J, Liu T. An adaptive thresholding algorithm for porosity measurement of additively manufactured metal test samples via X-ray computed tomography. Addit Manuf. 2021;39: 101899. http://doi.org/10.1016/j.addma.2021.101899.
58. Di Angelo L, Di Stefano P, Guardiani E. A review of computer-based methods for classification and reconstruction of 3D high-density scanned archaeological pottery. J Cult Herit. 2022;56:10–24. http://doi.org/10.1016/j.culher.2022.05.001.
59. Deseilligny MP, Clery I. Evolutions récentes en photogrammétrie et modélisation 3D par photo des milieux naturels. Collection EDYTEM Cahiers de géographie. 2011;12:51–66.
60. Athanasiou E, Faka M, Hermon S, Vassallo V, Yiakoupi K. 3D documentation pipeline of Cultural Heritage artifacts: A cross-disciplinary implementation. 2013 Digital Heritage International Congress (DigitalHeritage). Marseille, France: IEEE; 2013. p. 145–52. http://ieeexplore.ieee.org/document/6743724/. Accssed 6 Aug 2023. http://doi.org/10.1109/DigitalHeritage.2013.6743724
61. Pieraccini M, Guidi G, Atzeni C. 3D digitizing of cultural heritage. J Cult Herit. 2001;2:63–70. http://doi.org/10.1016/S1296-2074(01)01108-6.
62. Karami A, Battisti R, Menna F, Remondino F. 3D Digitization of transparent and glass surfaces: state of the art and analysis of some methods. Int Arch Photogramm Remote Sens Spatial Inf Sci. 2022;XLIII-B2–2022:695–702. http://doi.org/10.5194/isprs-archives-XLIII-B2-2022-695-2022.
63. Christie HR. Pushing boundaries: spectral imaging of archaeological small finds.
64. Fried P, Woodward J, Brown D, Harvell D, Hanken J. 3D scanning of antique glass by combining photography and computed tomography. Digital Appl Archaeol Cultural Herit. 2020;18:e00147. http://doi.org/10.1016/j.daach.2020.e00147.
65. Brancaccio R, Bettuzzi M, Casali F, Morigi MP, Levi G, Gallo A, et al. Real-time reconstruction for 3-D CT applied to large objects of cultural heritage. IEEE Trans Nucl Sci. 2011;58:1864–71. http://doi.org/10.1109/TNS.2011.2158850.
66. Kak AC, Slaney M. Principles of Computerized Tomographic Imaging. IEEE press. New York; 1999 [cited 2023 Aug 6]. https://doi.org/10.1137/1.9780898719277.

67. Schneider CA, Rasband WS, Eliceiri KW. NIH image to imageJ: 25 years of image analysis. Nat Methods. 2012;9:671–5. http://doi.org/10.1038/nmeth.2089.
68. Radchenko S, Dudok T. Metric field for scaling and measuring of the image-based 3D models. https://ukrpatent.org/uk/articles/bulletin-ip.
69. Nykonenko D. 3D models of glass beads from Khortytsia island. 2023, viewed 15 October 2023. https://sketchfab.com/dnykonen/models.
70. Zacharias N. Glass corrosion: issues and approaches for archaeological science. In: Fuxi G, editor. Recent advances in scientific research of glass and glaze. World Scientific: World Century. Singapore; 2016. p. 233–47.
71. Fiorentino S, Chinni T, Galusková D, Mantellini S, Silvestri A, Berdimuradov AE, et al. On the surface and beyond degradation morphologies affecting plant ash-based archaeological glass from Kafir Kala (Samarkand, Uzbekistan). Minerals. 2021;11:1364. http://doi.org/10.3390/min11121364.
72. Gulmini M, Pace M, Ivaldi G, Ponzi MN, Mirti P. Morphological and chemical characterization of weathering products on buried Sasanian glass from central Iraq. J Non-Cryst Solids. 2009;355:1613–21. http://doi.org/10.1016/j.jnoncrysol.2009.05.056.
73. Karklins K, Jargstorf S, Zeh G, Dussubieux L. The Fichtelgebirge Bead and Button Industry of Bavaria. BEADS: Journal of the Society of Bead Researchers. 2016;28:16-37. https://surface.syr.edu/beads/vol28/iss1/5.
74. Archaeological Museum SB UUSaT. bead N. 16. Scetchfab; 2019, viewed 15 October 2023. https://skfb.ly/oovSP.
75. Tait H. Five thousand years of glass. London: British museum press; 1991.

Publisher's Note